Dynamic Modeling of Floating Systems: Application to Eel-like Robot and Rowing system

Wisama Khalil*, François Rongère**
Ecole Centrale de Nantes, 1 Rue de la Noë, 44321 Nantes, France
*IRCCyN UMR CNRS 6597, ** LHEEA UMR CNRS 6598

***Abstract*—This paper presents the dynamic modeling of floating systems with application for three-dimensional swimming eel-like robot and rowing-like system. To obtain the Cartesian evolution during the design or control of these systems the dynamic models must be used. Owing to the complexity of such systems efficient and simple tools are needed to obtain their model. For this goal we propose an efficient recursive Newton-Euler approach which is easy to implement. It can be programmed either numerically or using efficient customized symbolic techniques**.

***Keywords*— Dynamic modeling, floating systems, Newton-Euler, recursive calculation, tree structure, eel-like robot, rowing like system.**

I. INTRODUCTION

This paper presents the dynamic modeling of floating systems with application for three-dimensional swimming eel-like robot and rowing-like system. The common characteristics of these structures are that there is no kinematic or geometric relationship between the Cartesian motion of the system and the joint variables. To obtain the Cartesian evolution of these systems the dynamic models must be used. For this goal we propose the generalization of the recursive Newton-Euler based algorithm of Luh and Walker [1] and of Featherstone [2] to these cases.

The recursive nature of the Newton-Euler approach provides efficient and easy to implement algorithms, which can be programmed either numerically or efficient customized symbolic programming techniques.

The paper is organized as follows: in section 2 we recall the method used to describe the kinematics of the structure which is based on the modified Denavit and Hartenberg conventions as proposed by Khalil and Kleinfinger, then in sections 3 and 4 we present the classical algorithm giving the inverse dynamic models of tree structure and closed loop rigid robots. The section 5 presents the generalization to the floating systems, sections 6 and 7 treat the applications on the eel-like serial robot and the closed loop rowing system. The conclusion constitutes section 8.

II. DESCRIPTION OF THE ROBOTS

The structures of the robots is described using Khalil and Kleinfinger notations [3]. This method can take into account tree structures and closed loop robots. Its use provide closed form solutions for the calculation of minimum number of inertial parameters [4], which reduce the number of operations of the dynamic models and are needed in the identification and adaptive control laws.

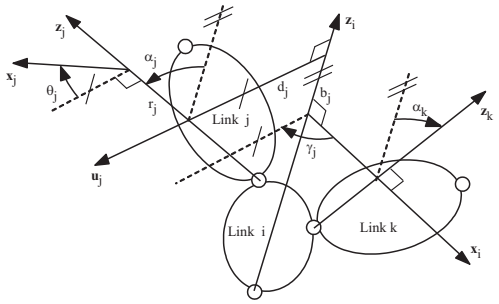

Figure 1: Geometric parameters for frame j.

A. Kinematic Description of Tree Structure Robots

A tree structure robot is composed of *n+1* links and *n* joints. Link *0* is the base, which can be fixed or mobile, and link *n* is a terminal link. The joints are revolute or prismatic, rigid or elastic. The links are numbered consecutively from the base, to the terminal links. Joint j connects link *j* to link *a(j)*, where *a(j)* denotes the link antecedent to link j. A frame R_i is attached to each link *i* such that (Figure 1):

- z_i is along the axis of joint *i*;
- $\boldsymbol{x_i}$ is along the common normal between z_i and one of the succeeding joint axes, selected on Figure 1 as z_k, the common normal between z_i and the other axes , as z_j on Figure 1, will be called u_j.

The transformation matrix ${}^{i}\underline{T}_{j}$, defining frame R_j with respect to (w.r.t) its antecedent frame R_i is obtained as a function of six geometric parameters $(\gamma_j,\ b_j,\alpha_j,d_j,\theta_j,r_j)$ such that:

$$ {}^{i}\underline{T}_{j} = Rot(z,\gamma_j)Tran(z,b_j)Rot(x,\alpha_j)Tran(x,d_j)Rot(z,\theta_j)Tran(z,r_j) $$

After developing, ${}^{i}\underline{T}_{j}$ can be written as:

$$ {}^{i}\underline{T}_{j} = \begin{bmatrix} {}^{i}R_j & {}^{i}P_j \\ 0_{1x3} & 1 \end{bmatrix} \qquad (1) $$

If x_i is along the common normal between z_i and z_j, both γ_j and b_j will be zero. This is always the case of serial structures. The type of the joint is identified by σ_j where $\sigma_j = 0$ if *j* is revolute, $\sigma_j = 1$ if *j* is prismatic, and $\bar{\sigma}_j = 1 - \sigma_j$. The joint

variable, denoted as q_j, is θ_j if j is revolute and r_j if j is prismatic. A serial structure is a special case of a tree structure where $a(j) = j-1, \gamma_j = 0, b_j = 0$ for all $j=1,..,n$.

B. Description of Closed Loop Structure

The system is composed of L joints and $n+1$ links, where link 0 is the base and $L > n$. The number of independent closed loops is equal to $B = L - n$. The joints are either active (motorized) or passive. The number of active joints is denoted N. The location of all the links can be determined as a function of the active variables. The geometric parameters are determined as follows:

i) Define the geometric parameters of the equivalent tree structure, with n joints and n+1 link, by cutting each closed loop at one of its passive joints as given in section II.A.

ii) Number the cut joints $k= n+1,...,L,$

iii) For each cut joint define two frames on one of the links connected by this joint. Assuming the links connected by the cut joint k are links i and j, the frames are defined as follows (Figure 2):

- frame R_k is fixed on link j such that $a(k)=i$, the axis z_k is along the axis of joint k, and x_k is along the common normal between z_k and z_j. The matrix ${}^{i}T_k$ is function of θ_k .
- frame R_{k+B} is aligned with R_k, but $a(k+B)= j$. The matrix ${}^{j}T_{k+B}$ is constant.

The joint variables of the system are denoted as:

- q_{tr} tree structure joint variables, q_c the cut joint variables,
- q_a, q_p active and passive joint variables of the tree structure

The geometric constraint equations for each loop k, for k=n+&,…,L, can be written as:

$$ {}^{k+B}\underline{T}_j \; ... \; {}^{i}\underline{T}_k \;\; = \;\; I_4 \tag{2}$$

The kinematic constraint equations are given by:

$$\begin{aligned} {}^{0}V_k &= {}^{0}V_{k+B} \\ \mathrm{J}_k \dot{q}_{b1} &= \mathrm{J}_{k+B} \dot{q}_{b2} \end{aligned} \tag{3}$$

Where V_k defines the (6×1) kinematic screw vector of frame k, given by:

$$V_k = \begin{bmatrix} v_k^T & \omega_k^T \end{bmatrix}^T \tag{4}$$

v_k linear velocity of the origin of frame R_k, ω_k angular velocity of frame k;

J_k the kinematic Jacobian matrix of frame k;

$\dot{q}_{b1}, \dot{q}_{b2}$ joint velocities through the two branches of the loop.

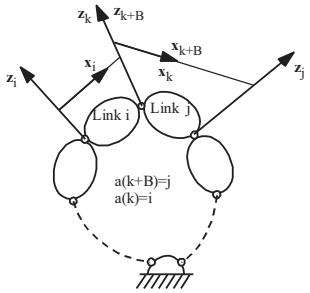

Figure 2: Frames around a cut joint k.

III. Dynamic Modeling of Tree Structure Robots With Fixed Base

A. Introduction

The most common methods used to calculate the dynamic models are the Lagrange equations and the Newton Euler Equations [5] [6]. The Lagrange model is given as:

$$\Gamma = A(q)\ddot{q} + h(q,\dot{q}) \tag{5}$$

where Γ is the joint torques, A is the inertia matrix of the robot and h is the Coriolis, centrifugal, external and gravity torques.

Calculating Γ in terms of $(\mathrm{q},\dot{\mathrm{q}},\ddot{\mathrm{q}})$ is the inverse dynamic problem, and calculating $\ddot{q}$ in terms of $(q,\dot{q},\Gamma)$ is known as the direct dynamic model. The inverse dynamic model is obtained from (5), whereas the direct model is calculated as:

$$\ddot{q} = (A)^{-1}(\Gamma - h) \tag{6}$$

The recursive Newton-Euler algorithms have been shown to be the most efficient technique to model rigid robots [1] [7] [8].

B. Calculation of the Inverse Dynamics Using Recursive N-E Algorithm

The algorithm consists of two recursive computations forward and backward [1]. The forward equations, from 1 to n, compute the velocities, accelerations and the wrench of the links. The backward equations from n to 1, provide the joint torques. The algorithm will be denoted by $\Gamma = \mathrm{NE}(q,\dot{q},\ddot{q},F_e)$, F_e is the external wrench exerted by the links on the environment.

-The forward equations for $j = 1,...,n$ are as follows:

$$ {}^{j}\omega_j = {}^{j}R_i \, {}^{i}\omega_i + \bar{\sigma}_j \, {}^{j}\underline{a}_j \, \dot{q}_j \tag{7}$$

$$ {}^{j}\dot{V}_j = {}^{j}T_i \, {}^{i}\dot{V}_i + \ddot{q}_j \, {}^{j}a_j + \begin{bmatrix} {}^{j}R_i\left[{}^{i}\omega_i \times \left({}^{i}\omega_i \times {}^{i}P_j \right)\right] + 2\sigma_j \left({}^{j}\omega_i \times \dot{q}_j \, {}^{j}\underline{a}_j \right) \\ \bar{\sigma}_j \, {}^{j}\omega_i \times \dot{q}_j \, {}^{j}\underline{a}_j \end{bmatrix} \tag{8}$$

$$ {}^{\mathrm{j}}\Phi_{\mathrm{j}} = {}^{j}I_{oj} \, {}^{j}\dot{V}_j + \begin{bmatrix} {}^{j}\omega_j \times \left({}^{j}\omega_j \times {}^{j}MS_j \right) \\ {}^{j}\omega_j \times \left({}^{j}\underline{I}_{oj} \, {}^{j}\omega_j \right) \end{bmatrix} \tag{9}$$

Where

- Φ_{j} total wrench on link j at origin of frame R_j;
- I_{oj} spatial (6×6) inertia matrix of link j around the origin O_j , which is given as:

$$I_{\text{oj}} = \begin{bmatrix} M_j I_3 & -{}^j M\hat{S}_j \\ {}^j M\hat{S}_j & {}^j \underline{I}_{oj} \end{bmatrix} \quad (10)$$

- $M_j, M\underline{S}_j, I_{oj}$ are the standard inertial parameters of link j. They are respectively, the mass, the first moments, and the (3×3) inertia matrix at the origin, $\hat{w}$ defines the skew matrix associated to the vector product such that; $w \times v = \hat{w}\, v$.

- $i = a(j)$, ${}^j\underline{a}_j = [0\ 0\ 1]^T$ unit vector along the joint axis (z-axis) referred to its own frame, ${}^j a_j = \left[0\ 0\ \sigma_j\ 0\ 0\ \bar{\sigma}_j\right]^T$,

- ${}^j T_i$ the (6×6) screw transformation matrix from frame j to frame i:

$${}^j T_i = \begin{bmatrix} {}^j R_i & {}^j \hat{P}_i\, {}^j R_i \\ 0_{3x3} & {}^j R_i \end{bmatrix} \quad (11)$$

In case of fixed base these equations are initialized by ${}^0\omega_0 = 0, {}^0\dot{\omega}_0 = 0$. The gravity effect on all the links is taken into account automatically by putting $\dot{v}_0 = -g$, with g is the gravity acceleration.

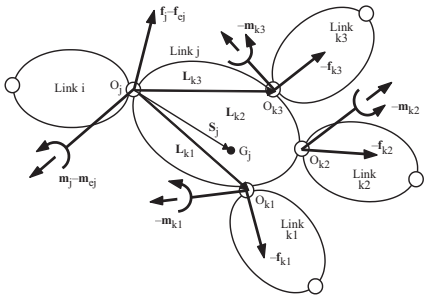

Figure 3: Forces and moments acting on link j.

The backward recursive equations are deduced from the total forces and moments on link j around its origin **(**Figure 3**).** They can be calculated for *j=n,...,1.*

$${}^{\text{j}}F_{\text{j}} = {}^{\text{j}}\Phi_{\text{j}} + \sum_k {}^{\text{k}}T_{\text{j}}^{\text{T}}\, {}^{\text{k}}F_{\text{k}} + {}^{\text{j}}F_{\text{ej}} \quad (12)$$

$$\Gamma_j = {}^{\text{j}}F_{\text{j}}^T\, {}^{\text{j}}a_{\text{j}} + I_{aj}\, \ddot{q}_j + F_{\text{sj}}\, sign(\dot{q}_j) + F_{\text{vj}}\, \dot{q}_j$$

Where $a(k) = j$, F_{j} is the reaction wrench (forces and moments) of link i on link j, F_{ej} is the wrench exerted by link j on the environment, Ia_j is the gear and rotor inertia of actuator j and F_{sj} , F_{vj} are friction parameters.

To reduce more the number of operations of the calculation of this model the base inertial parameters and the customized symbolic calculation can be used [7] [5]

C. Computation of the direct dynamic model

Two methods based on Newton-Euler methods can be used to obtain the dynamic model: the first is proposed by Walker and Orin [9], it is based on calculating the A and h matrices, defined in (5) using Newton-Euler inverse dynamic model and to calculate the joint accelerations by (6). The second method, which is devoted for tree structure robots and not applicable to closed loop robots, is based on a recursive Newton-Euler algorithm without calculating the inertia matrix [2][8]. The extension of the second method for floating robot systems will not be presented in this paper the interested reader can consult [12] .

IV. Dynamic Modeling of Closed Loop Robots

The computation of the Inverse dynamic model of closed loop robots can be obtained by first calculating the inverse dynamic model of the equivalent tree structure robot, in which the joint variables satisfy the constraints of the loop. Then the torques of the active joints of the closed loop torques Γ_c are obtained by solving the following equation:

$$\begin{bmatrix} \Gamma_c \\ 0 \end{bmatrix} = \Gamma_{\text{tr}}(q_{tr}, \dot{q}_{tr}, \ddot{q}_{tr}) + \text{W}^{\text{T}} \lambda \quad (13)$$

Where λ is the Lagrange multipliers and $W\dot{q}_{tr} = 0$ is the kinematic constraint equations between the velocities of the passive and active joints of the tree structure. The matrix W can be obtained from (3). After developing we obtain [10] [5][11]:

$$\Gamma_c = G^{\text{T}}\Gamma_{\text{tr}}(q_{tr}, \dot{q}_{tr}, \ddot{q}_{tr}) = \Gamma_a + \left(\frac{\partial \dot{q}_p}{\partial \dot{q}_a}\right)^T \Gamma_p \quad (14)$$

where:

$$G = \frac{\partial q_{tr}}{\partial q_a} = \frac{\partial \dot{q}_{tr}}{\partial \dot{q}_a} \quad (15)$$

Γ_a and Γ_p are the actuated and passive joint torques of the equivalent tree structure.

There is no recursive method to obtain the direct dynamic model of closed loop robots. It can be computed using the inverse dynamic model in order to obtain the matrices A_c and h_c such that [5]:

$$\Gamma_c = A_c(q_{tr})\ddot{q}_a + h_c(q_{tr}, \dot{q}_{tr}) \quad (16)$$

V. Dynamic Modeling of floating Robots

This section treats the floating robotics systems which are composed of a tree structure with moving base. It includes a big number of systems such as: mobile manipulators, walking robots, Humanoid robots, eel like robots [13][14] , snakes like robots, flying robots, spatial vehicles, offshore structures [17]. The main difference between these systems lies in the calculation of the interaction forces with the environment. In the previous sections the acceleration of the base is known and equal to zero, whereas in the case of moving base the acceleration of the base must be determined in both direct and inverse dynamic models. The motion of the system takes place thanks to the action- and reaction principle between the system and the environment. In general it cannot be determined by kinematic models except in the particular cases where the contact forces can be translated into constraints between the state variables of the system as in the case of non-holonomic wheeled mobile robots. The inverse dynamic model, which is used in general in the control problems, can be used in

simulation too when the objective is to study the evolution of the system giving joint positions, velocities and accelerations. The direct dynamic model can be used in simulation when the joint torques are specified. This model is not developed here.

The base frame R_0 is defined arbitrary fixed with link 0, its situation w.r.t the world fixed frame R_w is defined by the transformation matrix ${}^{w}\underline{T}_0$. This matrix is supposed known at t = 0, it will be updated by integrating the base accelerations. The velocity and acceleration of the base are represented by the (6x1) vectors V_0 and $\dot{V}_0$ respectively.

A. General Form of the Dynamic Models of Floating Systems

The dynamic model of a floating robot with n joints and moving base can be represented as follows:

$$\begin{bmatrix} 0_{6x1} \\ \Gamma \end{bmatrix} = A \begin{bmatrix} {}^{0}\dot{V}_0 \\ \ddot{q} \end{bmatrix} + h = \begin{bmatrix} A_{11} & A_{12} \\ A_{12}^T & A_{22} \end{bmatrix} \begin{bmatrix} {}^{0}\dot{V}_0 \\ \ddot{q} \end{bmatrix} + \begin{bmatrix} h_1 \\ h_2 \end{bmatrix} \quad (17)$$

At first, the base acceleration is obtained by using the first row of (17):

$${}^{0}\dot{V}_0 = -\left(A_{11}\right)^{-1}\left(h_1 + A_{12}\ddot{q}\right) \quad (18)$$

Then, the joint torques are obtained from the second row:

$$\Gamma = A_{12}^T\, {}^{0}\dot{V}_0 + A_{22}\,\ddot{q} + h_2 \quad (19)$$

The direct dynamic model gives the joint accelerations and the base acceleration in terms of the position and velocity of the base and the articulated system and the joint input torques. Thus using (17), the direct dynamic model is given as follows:

$$\begin{bmatrix} \dot{V}_0 \\ \ddot{q} \end{bmatrix} = A^{-1} \begin{bmatrix} -h_1 \\ \Gamma - h_2 \end{bmatrix} \quad (20)$$

The calculation of A and h by Lagrange is very time consuming for systems with big number of degrees of freedom (as the eel-like robot). Therefore, we propose to use a recursive method, which is easy to programme, and its computational cost is efficient [12] .

B. Recursive N-E Calculation of the Inverse Dynamics

The inverse dynamic algorithm in this case consists of three recursive steps (forward, backward, then forward) [13][12] .

-Forward recursive calculation:

In this step we calculate for $j = 1,...,n$ the following: ${}^{i}T_j$, ${}^{j}\omega_j$ as given in section (III.B). We calculate also ${}^{j}\beta_j$, ${}^{j}\gamma_j$, ${}^{j}\zeta_j$, appearing in the equations of total forces and link accelerations which are independent of the robot base acceleration ($\dot{v}_0, \dot{\omega}_0$):

$${}^{j}\beta_j = -{}^{j}F_{ej} - \begin{bmatrix} {}^{j}\omega_j \times \left({}^{j}\omega_j \times {}^{j}MS_j \right) \\ {}^{j}\omega_j \times \left({}^{j}\underline{Io}_j\, {}^{j}\omega_j \right) \end{bmatrix} \quad (21)$$

$${}^{j}\gamma_j = \begin{bmatrix} {}^{j}R_i \left[{}^{i}\omega_i \times \left({}^{i}\omega_i \times {}^{i}P_j \right) \right] + 2\sigma_j ({}^{j}\omega_i \times \dot{q}_j\, {}^{j}\underline{a}_j) \\ \bar{\sigma}_j\, {}^{j}\omega_i \times \dot{q}_j\, {}^{j}\underline{a}_j \end{bmatrix} \quad (22)$$

We define also:

$${}^{j}\zeta_j = {}^{j}\gamma_j + \ddot{q}_j\, {}^{j}a_j \quad (23)$$

-Backward recursive equations:

In this step we obtain the base acceleration using the inertial parameters of the composite link *0*, where the composite link j consists of the links articulated on it.

Using (9) and (12) the equilibrium equation of link j, can be rewritten as:

$${}^{j}F_j = {}^{j}I_{oj}\, {}^{j}\dot{V}_j - {}^{j}\beta_j + \sum_{k,a(k)=j} {}^{k}T_j^T\, {}^{k}F_k \quad (24)$$

Applying Newton-Euler equations on the composite link j, we obtain:

$${}^{j}F_j = {}^{j}I_{oj}^c\, {}^{j}\dot{V}_j - {}^{j}\beta_j^c \quad (25)$$

with:

$$\begin{aligned} {}^{j}I_{oj}^c &= {}^{j}I_{oj}^c + \sum_{k,a(k)=j} {}^{k}T_j^T\, {}^{k}I_{ok}^c\, {}^{k}T_j \\ {}^{j}\beta_j^c &= {}^{j}\beta_j^c + \sum_{k,a(k)=j} {}^{k}T_j^T \left({}^{k}\beta_k^c - {}^{k}I_{ok}^c\, {}^{k}\zeta_k \right) \end{aligned} \quad (26)$$

${}^{j}I_{oj}^c$ is the spatial inertial matrix of the composite link j.

For $j = 0$, and since ${}^{0}F_0$ is equal to zero, we obtain using (25):

$${}^{0}\dot{V}_0 = \left({}^{0}I_{o0}^c \right)^{-1} {}^{0}\beta_0^c \quad (27)$$

To conclude, the recursive equations of this step consist of initializing ${}^{j}I_{oj}^c = {}^{j}I_{oj}$, ${}^{j}\beta_j^c = {}^{j}\beta_j$ then calculate *for j = n,..., 1.*

$$\begin{aligned} {}^{i}I_{oi}^c &= {}^{i}I_{oi}^c + {}^{j}T_i^T\, {}^{j}I_{oj}^c\, {}^{j}T_i \\ {}^{i}\beta_i^c &= {}^{i}\beta_i^c + {}^{j}T_i^T \left({}^{j}\beta_j^c - {}^{j}I_{oj}^c\, {}^{j}\zeta_j \right) \end{aligned} \quad (28)$$

At the end ${}^{0}\dot{V}_0$ is calculated by (27).

- Second forward recursive equations:

After calculating ${}^{0}\dot{V}_0$, the wrench ${}^{j}F_j$ and the joint torques are obtained using (8) and (25) for j= 1,…, n as:

$${}^{j}\dot{V}_j = {}^{j}T_i\, {}^{i}\dot{V}_i + {}^{j}\zeta_j \quad (29)$$

$${}^{j}F_j = {}^{j}I_{oj}^c\, {}^{j}\dot{V}_j - {}^{j}\beta_j^c \quad (30)$$

$$\Gamma_j = {}^{j}F_j^T\, {}^{j}a_j + I_{aj}\,\ddot{q}_j + F_{sj}\, sign(\dot{q}_j) + F_{vj}\,\dot{q}_j \quad (31)$$

It is to be noted that the base linear acceleration is calculated by ${}^{0}\dot{v}_0 = {}^{0}\dot{v}_0 + {}^{0}g, \frac{d}{dt}{}^{0}v_0 = ({}^{0}\dot{v}_0 - {}^{0}\omega_0 \times {}^{0}v_0)$,. The integration of $\frac{d}{dt}{}^{0}v_0$ updates the new velocity ${}^{0}v_0$. After transforming it into frame w using the relation ${}^{w}R_0\, {}^{0}v_0$ and integration we obtain the new position. The integration of ${}^{0}\dot{\omega}_0$ permit to find the angular velocity ${}^{0}\omega_0$, after transforming it into frame w ${}^{w}R_0\, {}^{0}\omega_0$ then into Quaterion velocity or Euler Angles velocity and integration we obtain the new orientation.

VI. Dynamic Modeling of an Eel-like robot

A. Kinematic Model of the Robot.

In this section, we apply the algorithm of the previous sections for the simulation of an eel-like robot using Matlab and Simulink [13][19]. The robot is composed of 13 rigid bodies connected by 12 spherical joints. Each joint is represented by three intersecting revolute joints. This gives a system with 36 revolute joints and 37 links (Figure **4**). The first link (link 0), representing the head of the robot, is composed of a half of a spheroid and an elliptic cylinder. The links 3j-2 and 3j-1, for j=1,…12, are virtual zero mass links. The links 3j are elliptic cylinders and the last link, the tail, is constructed by a half of an ellipsoid Figure 5. The geometric parameters of the robot are given in table 1. The offset values q_{0j} are defined such that with q_j=0, the x_0 axis is aligned with the z_{3j} axes of the elliptical cylinder bodies (with j=1,…,12).

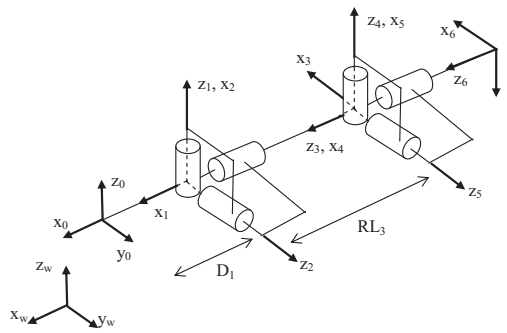

Figure 4: The 3D eel like robot

Table 1: Geometric parameters of the structure

j	α_j	d_j	θ_j	r_j	q_{0j}
1	0	0.4	θ_1	0	0
2	-π/2	0	θ_2	0	π/2
3	-π/2	0	θ_3	0.14	π/2
4	π/2	0	θ_4	0	-π/2
…					
35	-π/2	0	θ_{35}	0	-π/2
36	-π/2	0	θ_{36}	0.14	π/2

From Figure 4, we deduce that the local frame axes (e_{j1}, e_{j2}, e_{j3}) in which the fluid-structure model is defined are:

- For the head: $e_{01} = x_0 \quad e_{02} = y_0 \quad e_{03} = z_0$

- For links 3j: $e_{3j1} = z_{3j} \quad e_{3j2} = x_{3j} \quad e_{3j3} = y_{3j}$

The total length of the robot is 2.08 meter. The cross section is of elliptic shape (whose great axis length is equal to 18 cm and its small axis is equal to 13 cm). The half small and great axis's lengths of the elliptic section are denoted a and b respectively. The simulation is carried out firstly using the inverse dynamic model by giving the desired trajectory $q(t), \dot{q}(t), \ddot{q}(t)$ as inputs and ${}^0V_0(0) = 0$ as initial condition. To validate the direct dynamic model, the simulation has been carried out using as inputs the current state $q(t)$, $\dot{q}(t)$, ${}^0V_0(t)$ and $\Gamma(t)$ obtained from the inverse dynamic simulation. The two simulations gave the same results.

B. Calculation of Fluid-Structure Forces and Moments

We adopt a simple fluid mechanical model where the forces exerted by the fluid on a given link are supposed as being due to the motion of that link. Moreover the links are assimilated to elliptic cross-sectional cylinders whose serial assembly builds a shape variable cylinder with its axial length is about 10 times those of the transverse ones. Hence, we can invoke the slender-body theory of fluid mechanics. Based on this assumption, the fluid flow near the body can be replaced by a continuous slicing of planar flows transverse to the cylinders' axes. Hence, the fluid forces can be modelled by wrenches applied on each cross section of the links, which only depends of the transverse links' motion. This corresponds to the so-called strip-theory approach, commonly used in naval engineering [26].

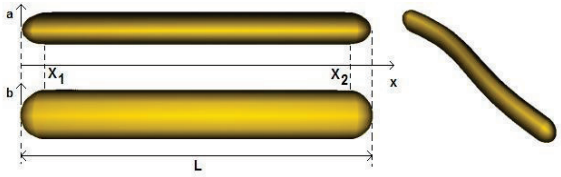

Figure 5: Geometry of the eel

To simplify the writing, we assume that the mass per unit of volume of the robot is equal to that of water such that the robot is neutrally buoyant. Moreover ${}^j v_j(s)$ denotes the velocity of a cross section of the link j positioned at the distance s along the link axis from the point O_j. This velocity can be decomposed in the local frame (e_{j1}, e_{j2}, e_{j3}) as:

$$ {}^j v_j(s) = v_{tj}(s) e_{j1} + v_{nj2}(s) e_{j2} + v_{nj3}(s) e_{j3} \tag{32} $$

where:

v_{tj} is the forward velocity component along axis e_{j1},

v_{nj2} and v_{nj3} are the perpendicular velocities along axis e_{j2} and e_{j3}. We also define: $v_{nj} = v_{nj2} e_{j2} + v_{nj3} e_{j3}$, and $\|v_{nj}\| = \sqrt{v_{nj2}^2 + v_{nj3}^2}$. Similar relations to (32) can be defined for ${}^j\dot{v}_j$.

The contact forces between the fluid and the cylindrical links of the eel can be obtained using Morison model [18], where the density of drag forces and moments along the links' axes and the density per unit of link axial length of added mass forces and torques are given respectively:

$$ {}^j f_{drag}(s) = C_{ld1,j} |v_{tj}(s)| v_{tj}(s) e_{j1} + \sum_{i=2}^{3} C_{ldi,j} \|v_{nj}(s)\| v_{nji}(s) e_{ji} \tag{33} $$

$$ {}^j m_{drag}(s) = C_{ad1,j} |\omega_{tj}| \omega_{tj} e_{j1} \tag{34} $$

$$ {}^{j}f_{am}(s) = \sum_{i=2}^{3} C_{lmi,j}\,\dot{v}_{nji}(s)\,e_{ji} \tag{35} $$

$$ {}^{j}m_{am}(s) = C_{am1,j}\,\dot{\omega}_{tj}\,e_{j1} \tag{36} $$

Where f_{drag} and m_{dragj} are due to the friction viscosity and pressure difference whereas f_{am} and m_{amj} are in relation with the quantity of fluid displaced during the movement. Finally the coefficients $C_{ldi,j}$, $C_{lmi,j}$, C_{ad1j} and C_{am1j} depend on the mass per unit volume of the fluid, the shape and size of the profile (here elliptic) and the Reynolds number of the moving profile in the fluid. Their values are given in [13].

The translational velocity and acceleration at a point whose curvilinear coordinate is s from the origin of frame j are calculated by:

$$ {}^{j}v_{j}(s) = {}^{j}v_{j} + {}^{j}\omega_{j} \times {}^{j}P_{j}(s) \tag{37} $$

$$ {}^{j}\dot{v}_{j}(s) = {}^{j}\dot{v}_{j} + {}^{j}\dot{\omega}_{j} \times {}^{j}P_{j}(s) + {}^{j}\omega_{j} \times {}^{j}\omega_{j} \times {}^{j}P_{j}(s) \tag{38} $$

Where ${}^{j}P_{j}(s)$ is the position of the s cross section with respect to the origin of the link fixed frame.

Superposing all the "slice-by-slice" contributions from $s = 0$ to $s = L_j$ (the axial length of the j[th] link), we find the global wrench exerted by link j on the fluid, expressed at O_j :

$$ {}^{j}F_{hj} = \begin{bmatrix} {}^{j}f_{hj} \\ {}^{j}m_{hj} \end{bmatrix} = \begin{bmatrix} {}^{j}f_{dragj} \\ {}^{j}m_{dragj} \end{bmatrix} + \begin{bmatrix} {}^{j}f_{amj} \\ {}^{j}m_{amj} \end{bmatrix} = \int_{0}^{L_j} {}^{j}F_{hj}(s)\,ds \tag{39} $$

where:

$$ {}^{j}F_{hj}(s) = \begin{bmatrix} {}^{j}f_{hj}(s) \\ {}^{j}m_{hj}(s) \end{bmatrix} = {}^{s}T_{j}^{T} \left(\begin{bmatrix} {}^{j}f_{drag}(s) \\ {}^{j}m_{drag}(s) \end{bmatrix} + \begin{bmatrix} {}^{j}f_{am}(s) \\ {}^{j}m_{am}(s) \end{bmatrix} \right) \tag{40} $$

$$ {}^{s}T_{j} = \begin{bmatrix} I_3 & -{}^{j}\hat{P}(s) \\ 0_{3\times3} & I_3 \end{bmatrix} \tag{41} $$

The drag and viscous wrench (39) is integrated numerically at each sample time of the algorithm from $s = 0$ to $s = L_j$, while the second contribution (added mass) can be explicitly computed in the local frame $(O_j, e_{j1}, e_{j2}, e_{j3})$ and transformed as constant element to be added to the spatial inertia matrix of the links such that:

$$ {}^{j}\mathrm{I}_{oj} = {}^{j}\mathrm{I}_{oj} + {}^{j}\mathrm{I}_{oj}^{aj} \tag{42} $$

C. *Simulation results*

In this example, we study the planar forward propulsion. Following bio-mechanic's literature about anguilliform locomotion [20],[19],[21], a planar forward propulsion motion is produced by a continuous motion law of the following form:

$$ Q(s,t) = f(t).A.e^{\alpha.s}.\sin\left[2\pi\left(\frac{s}{\lambda} - \frac{t}{T}\right)\right] + off_1 \tag{43} $$

where A is the amplitude of the motion, α is introduced to increase the amplitude when going from the head to the tail [21], $1/T$ is the frequency of the wave, λ represents the length of the wave, and s the curvilinear coordinate along eel's backbone. The function $f(t)$ is a smoothing function of fifth degree polynomial such that:

$f_1(0) = 0$, $f_1(t_f) = 1$, $\dot{f}_1(0) = \ddot{f}_1(0) = 0$, $\dot{f}_1(t_f) = \ddot{f}_1(t_f) = 0$

and off_1 is a constant used to carry out the deviation,

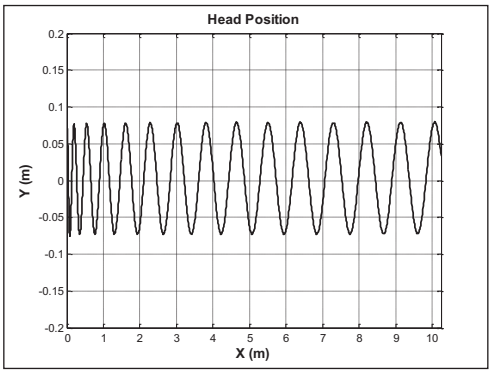

Figure 6: Head's trajectory in the **x**-**y** plane of the fixed world frame.

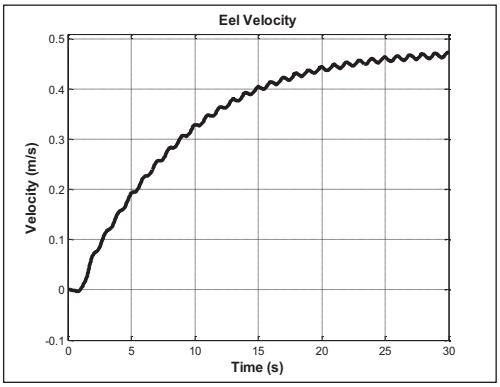

Figure 7: Velocity of the head with respect to time.

To apply this continuous motion law, we have to discretize equation (43) to obtain the corresponding value on each joint [24]. The values of the first joints of the spherical joints (joints numbered $j = 3i - 2$, with $i = 1,...,12$ denotes the number of the spherical joint) are:

$$ q_j(t) = Q(X_{j+1}, t) - Q(X_j, t) \tag{44} $$

where $X_j = \sum_{k=1}^{j} r_k$ is the distance of each joint from the head

The other joint angles are taken equal to the constant offset given in Table 1. The following numerical values are used:

$$ A = 0.06\,,\ \alpha = 1.2\,,\ \mathrm{t_f} = 2\,\mathrm{s}\,,\ \lambda = 1.8\,\mathrm{m}\,,\ \mathrm{T} = 2\mathrm{s}\,,\ off_1 = 0 $$

Figure 6 shows the head trajectory of the eel in the xw-yw plane of the fixed world frame for a simulation of 30s. Figure 7 gives the linear forward velocity of the robot in the *fixed world*

frame. These results show that the eel has a straight line trajectory with a small transversal oscillatory motion. The eel needs approximately 30s to reach its final speed, in order to satisfy the limits of actuators torques ($\pm 4N.m$ for joints 3j-2 and 3j-1, and $\pm 0.7N.m$ for joints 3j).

VII. Dynamic Modeling of a Rowing-like system

A. Kinematic Model of the Rower-Oars-Boat system

In this section we apply the algorithm for the simulation of a boat-oars-rower system. Figure 8 shows the model of the rowing system. As shown, rower is modeled with three rigid bodies connected by revolute joints: two for the legs and one for the trunk. Both oars are connected to the boat by revolute joints (oarlocks). The rower is connected to the boat via the foot stretcher and to the sliding seat, both with revolute joints. The sliding seat is connected to the boat via a prismatic joint. Vocabulary used here is defined Figure 9. The geometric parameters of the model are presented in Table 2. Geometric parameters as well as principal inertia parameters of each rigid body of the rower have been extrapolated from De-Leva [29]. Concerning the boat and oars, we took measurement data on a real single skull (a one person boat). Beside the inertia parameters, riggings of the boat and oars have been measured on real material. They represent the position and height of the foot stretcher (d_1 and b_1), the height of the sliding seat (b_4), the position of the oars in the boat (d_5 and d_6) and the external lever of the oars (L_e).

For the sake of simplicity, arms of the rower are not modeled as it would introduce two loop closure constraints. Nevertheless this model embeds one loop composed of the legs, the sliding seat and the boat. This impose that we have to choose which joints are driven in the loop. Table 2 introduces the variable μ_j in order to indicate active and passive joints by taken the value 1 and 0, respectively. Active joints are explicitly driven whereas passive joint trajectories are determined from loop closure constraints.

The boat is floating in six degree of freedom, but it is constrained to remain in the vertical plane of its advance direction. Hence it can move following surge, heave and pitch. Its complex motion result from the alternative propulsion by oars, the motion of the rower and the interaction of the boat and water. Hydrodynamic models for the boat and oars interaction with water are exposed hereafter.

B. Rowing Forces Models

A summary of the nature of the forces exerted on the rowing system is made here. Hull hydrodynamics as well as oars hydrodynamics are considered via physical models.

1) Hull hydrodynamics

Interactions between the boat hull and water are developed here. Forces induced on the hull by water are considered to be of three kind and only apply on the boat.

$$ {}^0F_{hyd_0} = {}^0F_{hs_0} + {}^0F_{rad_0} + {}^0F_{v_0} \quad (45) $$

${}^0F_{hyd_0}$, ${}^0F_{rad_0}$ and ${}^0F_{v_0}$ are respectively the hydrostatic forces, the radiation forces and the viscous forces.

a) Hydrostatic forces:

The hydrostatic forces also known as buoyant forces are considered as being linear with respect to the boat position and orientation at rest defined in the inertial frame. They can be expressed as follow:

$$ {}^0F_{hs_0} = \begin{bmatrix} {}^0R_w & 0_{3\times3} \\ 0_{3\times3} & {}^0R_w \end{bmatrix} G\eta \quad (46) $$

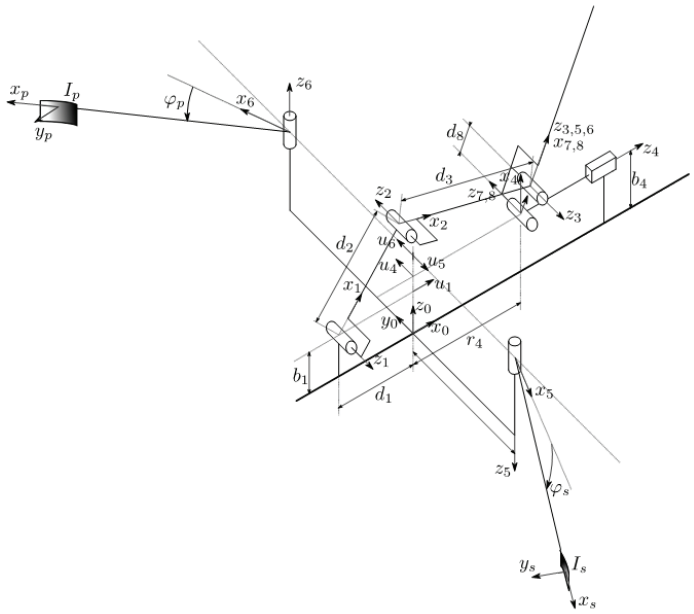

Figure 8: Model of the rowing system

Table 2: Geometric parameters of the rowing system

j	a(j)	μ_j	σ_j	γ_j	b_j	α_j	d_j	θ_j	r_j
1	0	0	0	0	b_1	$\pi/2$	$-d_1$	θ_1	0
2	1	1	0	0	0	π	d_2	θ_2	0
3	2	1	0	0	0	π	d_3	θ_3	0
4	0	0	1	$\pi/2$	b_4	$\pi/2$	0	$\pi/2$	r_4
5	0	1	0	$-\pi/2$	b_5	π	d_5	θ_5	0
6	0	1	0	$\pi/2$	b_6	0	d_6	θ_6	0
7	4	0	0	0	0	$\pi/2$	0	θ_7	0
8	3	0	2	0	0	π	$-d_8$	0	0

Where G is the 6×6 stiffness matrix of the hull. Stiffness is only present for motions of heave, pitch and roll thus the only non-zero coefficients of G are those with $i,j \in \{3,5,6\}$. η is the Cartesian position and the Cardan angles ((ψ,θ,ϕ)) of the boat with respect to the world fixed frame . The relation

between the boat speed expressed in its frame and $\dot{\eta}$ is given by:

$$\dot{\eta} = \begin{bmatrix} {}^{w}R_0 & 0_{3\times3} \\ 0_{3\times3} & {}^{w}\Omega_0 \end{bmatrix} {}^{0}V_0 \tag{47}$$

$${}^{w}\Omega_0 = \begin{bmatrix} 1 & S\phi T\theta & C\varphi T\theta \\ 0 & C\phi & -S\phi \\ 0 & S\phi/C\theta & C\phi/C\theta \end{bmatrix} \tag{48}$$

Where S, C and T denote sin, cos and tan respectively.

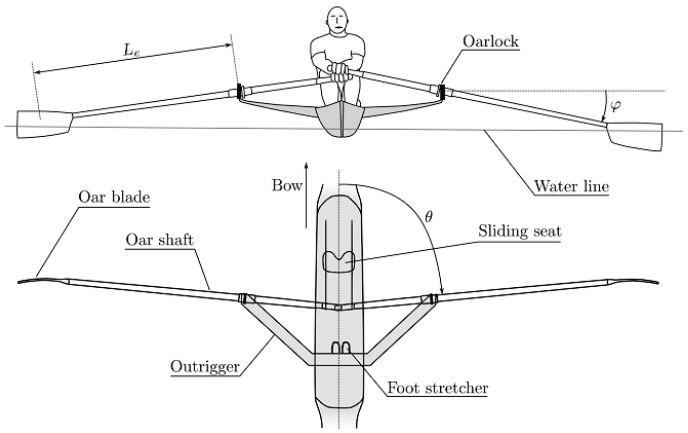

Figure 9: Front and top view of the rower with principal links

b) Radiation forces

The radiation forces are related to the secondary motions of the boat superimposed to the steady forward motion. These secondary motions are due to the unsteady interaction between the rower and the boat as well as the alternative propulsive excitation made by the oars. They induce a wave field radiated around the boat towards the infinity which modifies the system dynamics and add some extra energy consumption. The latter is due to free surface effects produced by the interaction between the oscillating floating body and the water. By considering little motions around the steady forward motion the radiation can be modeled in a linear framework. The potential flow theory lead to an expression composed of two parts. The first is proportional to the acceleration and is related to an added mass. The second is proportional to the velocity of the boat and is named the potential damping. The radiation forces are written:

$${}^{0}F_{rad_0} = -A(\omega)\,{}^{0}\dot{V}_0 - B(\omega)\,{}^{0}V_0 \tag{49}$$

Where $A(\omega)$ and $B(\omega)$ are respectively the added mass and potential damping matrices. These matrices depend on the frequency ω of the motion. The issue is that the frequency content of the boat speed and acceleration is not known at the simulation runtime because the latter quantities are unknown of our problem. Cummins [30] shows that the radiation forces can be expressed in the time domain as:

$${}^{0}F_{rad_0} = -A_\infty\,{}^{0}\dot{V}_0 - B_\infty\,{}^{0}V_0 - \int_0^t K(t-\tau)\,{}^{0}V_0(\tau)d\tau \tag{50}$$

where $A_\infty = \lim_{\omega\to\infty} A(\omega)$ and $B_\infty = \lim_{\omega\to\infty} B(\omega)$ are the constant infinite frequency added mass and potential damping matrices and the convolution term represents the fluid memory effects. The 6x6 convolution kernel matrix K is the impulse response or retardation functions [31]. The impulse response along each mode of motion and coupled modes are obtained from the seakeeping code AQUAPLUS [32] applied to a meshed rowing boat hull. However the computation of the convolution term is computationally expensive as it integrates over the whole period of simulation. A powerful way to calculate it is to use a state-space representation [33] such that:

$$\begin{aligned} \dot{x}(t) &= \underline{A}x(t) + \underline{B}\,{}^{0}V_0 \\ \int_0^t K(t-\tau)\,{}^{0}V_0(\tau)d\tau &\approx \underline{C}x(t) \end{aligned} \tag{51}$$

where x is the state vector of the boat.
This lead to an augmented set of ordinary differential equations for solving both multibody dynamics and hull radiation model.

c) Hydrodynamic resistance:

It is expressed in a basic form following ITTC'57 [34] formulation:

$${}^{0}F_{v_0} = \begin{bmatrix} -\frac{1}{2}\rho S C_t V_x^2 & 0_{1\times5} \end{bmatrix}^T \tag{52}$$

with $C_t = (1+k)C_f + C_w$, k the form coefficient, C_w the wave resistance coefficient, $C_f = \dfrac{0.075}{\left(\log_{10} R_e - 2\right)^2}$ the friction coefficient, R_e the Reynolds number. V_x is the x-component of the boat speed ${}^{0}V_0$. S and L, respectively the wetted surface and the boat length, are considered constant. For the simulation presented hereafter, we took $k = 1$ and $C_w = 0.1C_f$ from model basin trials.

2) Oar hydrodynamics

As the simplified model does not involve arms, interaction between oars and the rower are not considered but their motions are independently but realistically specified.
For the example shown here, the modeling of the propulsion force is the simplest one, *i.e* a force normal to the blade and proportional to the square of the normal component of the absolute velocity at the center of the blade.

The water velocity on the blade can be calculated by (j=5,6):

$${}^{j}v_{flow_j} = {}^{j}v_{I_j\,j} = -{}^{j}v_j + O_jI_j \times {}^{j}\omega_j = \begin{bmatrix} v_t & v_n & 0 \end{bmatrix}^T \tag{53}$$

where v_n and v_t $\mathrm{v_t}$ are respectively the normal and tangential components of the flow speed seen by the blade at point I_j.

We define the angle φ_j for each oar corresponding to the inclination of the oar shaft with the local horizontal plane of the boat. With the convention adopted in the model Figure 8, we have $\varphi_6 = -\varphi_5 > 0$. Hence the position of the point I_j where the hydrodynamic forces are considered to apply can be calculated by

$$O_j I_j = \begin{bmatrix} L_e C\varphi_j & 0 & -L_e S\varphi_j \end{bmatrix}^T \quad (54)$$

where L_e is the external lever as defined Figure 9. According to [35] the normal forces are expressed by:

$$F_n = \frac{1}{2}\rho S C_n v_n |v_n| \quad (55)$$

where C_n is the normal force coefficient ($C_n = 2$), ρ the water mass density and S the projected area of the blade. Finally the force model to apply on oars can be expressed by

$${}^j f_{oar_j} = \begin{bmatrix} 0 & F_n & 0 \end{bmatrix}^T \quad (56)$$

$${}^j F_{oar_j} = \begin{bmatrix} {}^j f_{oar_j} \\ O_j I_j \times {}^j f_{oar_j} \end{bmatrix} \quad (57)$$

The propulsive wrench on the blade is cancelled as soon the normal flow velocity v_n becomes positive.

C. Motion Generation

Because it is more easy to measure human joint angles than joint torques, the inverse dynamic model has been adopted for the rowing simulation. In this case each active joint trajectory q_j has to be specified with its first and second derivative. A motion generator specially developed for rowing has been developed to generate and adjust motion models for the actuated joints. It consists of an interface allowing for interactive manipulation of periodic B-Spline curves to model each of the joints trajectories on one rowing stroke. The B-Spline control polygon is used to deform curves by hand.

As for the human motion, joints trajectories have to be smooth. The smoothness is essential to avoid unwanted oscillations in the system. As a matter of fact, discontinuity in acceleration is seen as a chock by the system which is essentially a spring damper system concerning hull hydrodynamics. Hence, to ensure this smoothness, degree 3 B-splines have been used. Continuity has also to be verified at the boundaries of the motion models on one period of motion which lead to periodic motion. Figure 10 shows an example of two set of joints trajectories generated for the rowing model.

D. Simulations

Although the algorithms presented deals with the six degree of freedom of the base, we just kept the surge, heave and pitch motions for simplicity. Two different motion sets are used in order to compare for the influence on the boat dynamics. Both are for a stroke rate of 27spm (period 22s). The difference is the ratio between the drive (propulsive) and the recovery (oars out of water) phases of the rowing stroke. The ratio is respectively 40% and 50% for the first and second set. The generation of the two motions is made by deforming B-spline curves for active joints variables by hand with the help of the control polygon.

Figure 10 shows the different active variables for the two sets of motion. Figure 11 gives the linear forward velocity on one period of motion. Figure 12 and Figure 13 show respectively the heave and pitch motions. Figure 10 shows that we changed the drive/recovery ratio by modifying the time of the maximum from 0.89s to 1.11s. It may reflect two rowing techniques. The influence on boat velocity is clear on Figure 11 and we can see that the velocity fluctuation is modified as well as the mean boat forward speed (4.28m/s vs. 4.03m/s). We superimposed an on-water measured velocity of a single skull rowing boat at the same stroke rate to verify for consistence of simulation. It appears on Figure 11 that the first motion (ratio 40%) better follows the experimental data while measurements also approximately sowed a 40% ratio and a mean forward velocity of 4.29m/s which is in a good accordance with our first simulation. The comparisons on Figure Figure 12 and Figure 13 of the zero mean secondary motions exhibit smaller secondary motions in favour of the second motion.

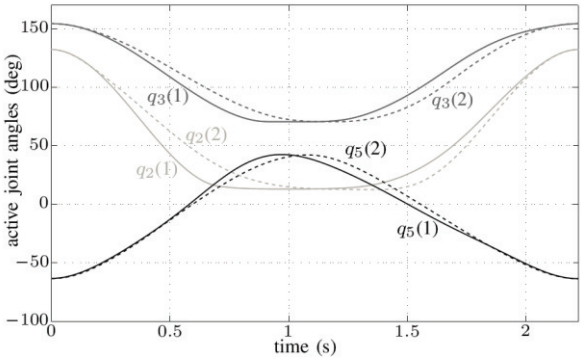

Figure 10: q_2 (knee angle), q_3 (trunk angle) and q_5 (starboard oar angle) for both motions

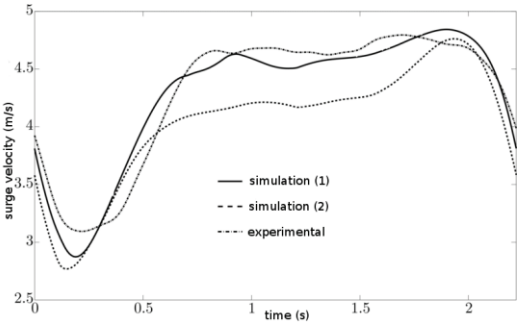

Figure 11: Surge velocity of the boat for the two motions compared with experimental data at 27spm

VIII. Conclusion

This paper presents the inverse and direct dynamic modelling of floating multi-body systems. The inverse dynamic model is developed using the recursive Newton-Euler algorithms. It provides the acceleration of the base beside the torque of the joints. The inverse dynamic model is used here to simulate two different systems the eel-system has a serial

structure with 36 joints, and the rowing-system has a closed loop structure. The proposed algorithms have been generalized for micro continuous system [19], and flexible flying structure [36].

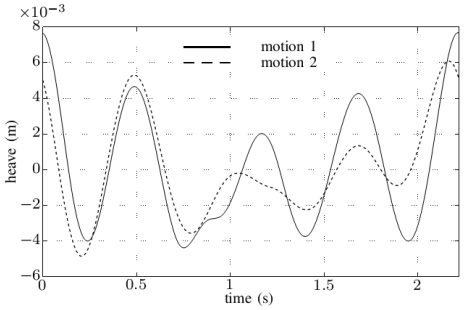

Figure 12: Heave motion of the boat for both motions

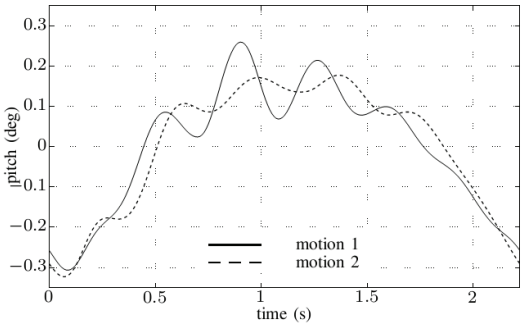

Figure 13: Pitch motion of the boat for both motions

REFERENCES

[1] J.Y.S Luh, M.W. Walker, and R.C.P. Paul, "On-line computational scheme for mechanical manipulators". *Trans. of ASME, J. of Dynamic Systems, Measurement, and Control*, Vol. 102(2) pp. 69-76, 1980

[2] R. Featherstone, "The calculation of robot dynamics using articulated-body inertias", *Int. J. of Robotics Research,* vol. 2(3), pp. 87-101,1983

[3] W. Khalil, and J.-F Kleinfinger, "A new geometric notation for open and closed-loop robots", *Proc. IEEE Int. Conf. on Robotics and Automation, San Francisco,* pp. 1174-1180. 1986.

[4] W. Khalil, and F. Bennis, "Symbolic calculation of the base inertial parameters of closed-loop robots". *International Journal of Robotics Research,* vol 14, n°2, pp. 112-128, 1995.

[5] W. Khalil, and E. Dombre, Modeling identification and control of robots. Hermes, Penton-Sciences, London, 2002.

[6] J. Angeles, Fundamentals of Robotic Mechanical Systems. Second edition, Springer-Verlag, New York, 2002.

[7] W. Khalil, and J.-F Kleinfinger, "Minimum operations and minimum parameters of the dynamic model of tree structure robots", *IEEE J. of Robotics and Automation,* vol. RA-3(6), pp. 517-526, 1987.

[8] W. Khalil and D. Creusot, "SYMORO+: a system for the symbolic modelling of robots", *Robotica*, vol. 15, pp. 153-161, 1997.

[9] M.W.Walker and D.E. Orin, "Efficient dynamic computer simulation of robotics mechanism", *Trans. of ASME, J. of Dynamic Systems, Measurement, and Control,* vol. 104, pp. 205-211, 1982.

[10] J.-F.Kleinfinger , and W. Khalil, "Dynamic modelling of closed-chain robots", Proc. 16th *Int. Symp. on Industrial Robots,* Bruxelles, pp. 401-412, 1986.

[11] Y. Nakamura, M Ghodoussi , "Dynamics computation of closed-link robot mechanisms with nonredundant and redundant actuators", *IEEE Transactions on Robotics and Automation*, Vol. 5 (3), p.294-302, June 1989.

[12] W.Khalil, « Dynamic modeling of Robots using Newton-Euler Formulation", *Lecture Notes in Electrical Engineering 89, Informatics in Control, Automation and Robotics,* J.A.Cetto, J-L Ferrier, J. Filipe (editors), 2010, pp. 3-20, Springer, 2010.

[13] W. Khalil, G. Gallot, and F. Boyer, "Dynamic Modeling and Simulation of a 3-D Serial Eel-Like Robot." *IEEE Transactions on Systems, Man and Cybernetics, Part C: Application and reviews,* vol. 37, N° 6. pp.1259-1268, 2007.

[14] K.A. McIsaac and J.P. Ostrowski, , "A geometric approach to anguilliform locomotion modelling of an underwater eel robot," *IEEE Int. Conf. Robotics and Automation,* pp. 2843-2848, 1999.

[15] J.P. Ostrowski and J.W. Burdick, "The geometric mechanics of undulatory robotics locomotion," *The international journal of robotics research,* vol.17, No.7, pp.683-701. 1998.

[16] R. Mason and J.W. Burdick, "Experiments in caranguiform robotic fish locomotion," *IEEE Int. Conf. Robotics and Automation*, pp. 428-435, 2000.

[17] F. Rongère, A.H. Clément, "Systematic dynamic modeling and simulation of multibody offshore structures : Application to wave energy converters", *ASME 2013 32nd Int. Conf. on Ocean, Offshore and Artic Engineering,* June 2013.

[18] J.R. Morison and al., "The force exerted by surface waves on piles," Transaction of the AIME, 189, pp.149-154, 1950.

[19] F. Boyer, Porez and W. Khalil, "Macro-continuous torque algorithm for a three-dimensional eel-like robot", *IEEE Robotics transaction,* vol.22, No.4, pp. 763-775, 2006

[20] G.B. Gillis, "Environmental effects on undulatory locomotion in the american eel anguilla rostrata: kinematics in water and on land," J. of Experimental Biology, 201, pp.949-961, 1998.

[21]E.D. Tytell and G.V. Lauder, "The hydrodynamics of eel swimming: I. Wake structure," J. of Experimental Biology, 207, pp.1825-1841, 2004.

[22] E.J. Kim and Y. Youm, "Design and dynamic analysis of fish robot: PoTuna," *IEEE Conf. On Robotics and Automation*, New Orleans, LA, pp.4887-4892, April 2004.

[23] J. Lighthill, "Large-amplitude elongated-body theory of fish locomotion*," Proc. R. Soc. Lond,* Ser. B179, pp.125-138, 1971.

[24] J. Yu, S. Wang and M. Tan, "A simplified propulsive model of bio-mimetic robot fish and its realization," *Robotica*, vol.23, pp. 101-107, 2005.

[25] S.F. Galls, Development of a computational model for an underwater autonomous vehicle, PhD thesis Texas A&M University, 2001.

[26] E.V. Lewis, Principles of naval architecture volume III motion in waves and controllability, The Society of Naval Architects and Marine Engineers, 1989.

[27] J. Katz and A. Plotkin, Low Speed Aerodynamics, Cambridge Univ. Press, second. ed., 2002.

[28] G. Susbielles and Bratuch, Vagues et ouvrages pétroliers en mer, Editions Technip, 1981.

[29] P. De-Leva, "Adjustments to Zatsiorsky-Seluyanov's segment inertia parameters", *Journal of Biomechanics,* vol. 29, no. 9, pp. 1223-1230, 1996

[30]W. Cummins, "The impulse response function and ship motions", Department of the Navy, David Taylor Model Basin, Seaworthiness and Fluid Dynamics Division Report 1661, Tech. Rep., 1962

[31] T. Ogilvie, "Recent progress taword the understanding and prediction of ship motions", in Fifth Symposium on Naval Hydrodynamics, vol. 112, 1964

[32] G. Delhommeau, "Seakeeping codes AQUADYN and AQUAPLUS", *in Offshore Structures : 19th WEGEMT School,* 1993

[33] E. Kristiansen, A. Hjulstad, and O. Egeland, "State-space representation of radiation forces in time-domain vessel models", Ocean Engineering, vol. 32, no. 17-18, pp. 2195-2216, 2005

[34] J.B. Hadler, "Coefficients for International Towing Tank Conference 1957 model-ship correlation line", Tech. Rep., DTIC Document, 1958

[35] J. Wellicome, "Some hydrodynamic aspects of rowing", in Rowing: a scientific approach, A symposium, 1967.

[36] A.Belkhiri, "Modélisation dynamique de la locomotion compliante : Application au vol battant bio-inspiré de l'insecte", Ph.D thesis, EMN, Nantes, 2013.